

Sensitivity enhanced photo-thermal borders detection in bio-phantoms enriched with gold nanoparticles

Yossef Danan^{1,2}, Ariel Schwarz^{1,2}, Moshe Sinvani^{1,2}, Zeev Zalevsky^{1,2*}

¹Faculty of Engineering, Bar-Ilan University, Ramat-Gan, 5290002, Israel

²Institute for Nanotechnology and Advanced Materials, Bar-Ilan University, Ramat-Gan, 5290002, Israel

*Corresponding author

DOI: 10.5185/amlett.2018.1860

www.vbripress.com/aml

Abstract

In the last decade diversity of applications in the fields of diagnostics and treatment for biomedical applications using gold nanoparticles (GNPs) as contrast agent sprang up. The strong optical absorption and scattering properties of the GNPs due to their localized surface plasmon resonance (LSPR) effect enables their use as contrast agents in these applications. The usage of the light-scattering properties of the GNPs in most imaging methods lead to background noise stems from light scattering from the tissue due to the same wavelengths of the illumination source and the GNPs' scattering. In our previous works we presented a method to improve border detection of bio-phantoms enriched with GNPs leading for real-time complete tumor resection by using a modulated laser illumination, photo thermal imaging camera and the optical absorption of specially targeted GNPs. In this system the thermal camera detects the temperature field of the illuminated bio-phantoms. Although the surrounding area got heated the border location was detected at a precision of at least 0.5 mm through use of a simple post processing technique. In this paper, we present a continuation of our previous research with modified system of time sequence labelling (TSL) processing for improved border detection capable of operating and detecting borders at much lower signal to noise levels. Copyright © 2018 VBRI Press.

Keywords: Photo thermal imaging, gold nanoparticles, localized surface plasmon resonance, image processing.

Introduction

One of the main problems in cancer resection surgeries is the recurrence of the disease after tumor resection surgery. In order to prevent a local recurrence of the disease and a reoperation procedure, a complete excision is critical. Currently, following the surgical procedure, routine histological tests are usually done for tumor margins examinations. Through the past few years, a few intraoperative tumor margin detection methods have been developed with some success. However, a highly sensitive and specific intraoperative tumor margin detection technique is still required that will decrease the recurrence of the cancer and the need of repeated medial operation. This high sensitivity detection is much more crucial when the cancerous tissue growth nearby neurological systems, and it is hazardous to resect an extra tissue [1]. Over the years, various techniques have been developed for better tumor margins visualization, such as: CT [2], MRI [3] and fluorescence imaging [4]. However, those methods have limited resolution derived from tissue displacement during operation [5], and other problems [6–8].

Gold nanoparticles (GNPs) have been used as biomarkers by numerous research groups not only as imaging contrast agents [9,10] but also for other biomedical applications such as drug delivery [11] and

therapeutics [12,13]. GNPs have been used as photo thermal therapy-mediated agents because their properties of photo-stability and biocompatibility [14] as well as the LSPR which causes high optical absorption and scattering cross-sections [15]. Illuminating the GNPs with a wavelength in correspondence to the LSPR will cause a strong oscillation of the free electrons in the nanoparticles. These strong oscillating motions will result an optical absorption and scattering amplifications [16,17]. The light scattering properties are necessary for imaging techniques based on light-scattering modalities [18] while the light absorption properties are utilized in photo thermal therapy and bright field microscopy [19], for instance. The GNP's size, the refractive indices of the GNP and its surrounding determine the resonance wavelength. In our previous research we showed a photo thermal imaging method by using modulated laser beam illumination on phantom enriched with targeted gold nanorods (GNRs) and a photo thermal imaging camera [20,21]. The GNRs absorb the optical energy of the illuminations which changes into temperature elevation of the GNRs and distribute to their vicinity when it is illuminated with a wavelength in correspondence to the LSPR wavelength. These particles are specifically targeted to attach the surface of cancer cells. Therefore, the temperature change happens inside the tumor [22–24]. This gives us an opportunity to differentiate between

noncancerous and cancerous tissues using a thermal imaging technique. The usage of continuous-wave (CW) laser cause a problem of continually elevated temperature and dissipated out of the GNPs' area. This heat dissipation affects the accuracy of border detection.

In our system, a modulated laser was used, in order to decrease the heat dissipation to noncancerous tissues and to increase the ability to detect the tumor borders. An increasing of the margins detection spatial resolution and the signal to noise ratio (SNR) was accomplished by applying, in each heating cooling cycle, a subtraction between the maximal and minimal thermal maps (even with the overall temperature elevation). The background noise which stems from light scattering from the tissue was prevented using photo thermal imaging unlike in commonly used imaging methods based on light-scattering techniques. The result is higher contrast between the healthy tissue and the cancerous cells and improved SNR.

In this paper we present an improved concept based upon time sequence labeling (TSL) processing for improved border detection capable of operating and detecting borders at much lower levels of SNR.

Experimental setup

The experiment was aimed to process the obtained thermal map over samples during laser illumination by a photo-thermal camera (FLIR, model A325). This photo-thermal camera can detect thermal emission at optical wavelengths of 8–14 μ m, and thus is blind to the laser illumination. The camera has temperature sensitivity of 0.07°C and 320 \times 240 pixels. The spatial resolution of the camera is 0.5mm per pixel.

One can see in **Fig. 1** an illustration of the experimental setup. In the experiments a near infra-red (NIR) laser at optical wavelength of 808nm and 1.6 W/cm² maximal power density was utilized. The NIR illumination was at a wavelength in adjacent to the LSPR wavelength of the GNPs that were utilized. The experiments were done in this wavelength region due to the greatest penetration depth of light into biological tissues it provides. This laser source was modulated in order to create different duty-cycles and frequencies of a square wave by a function generator (AFG3022B by Tektronix).

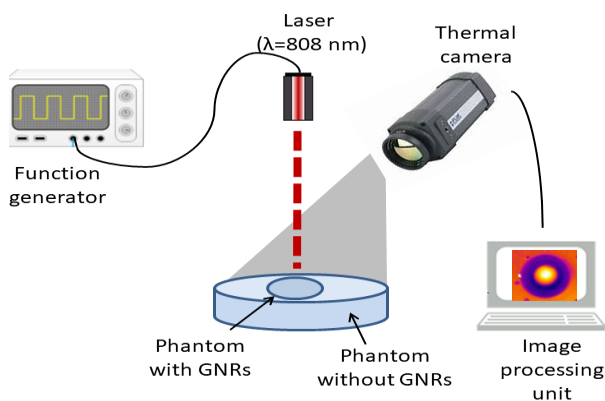


Fig. 1. An illustration of the experimental setup.

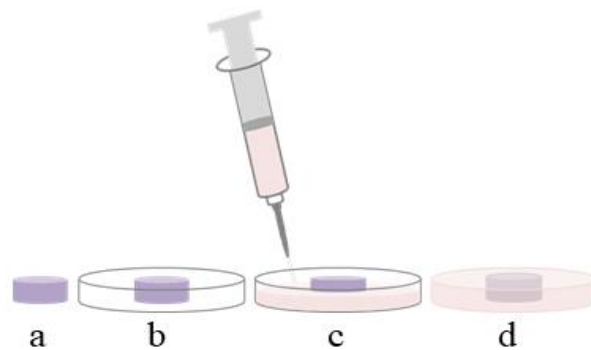


Fig. 2. The combined solid tissue like phantom preparation process.

Results and discussion

Solid tissue-like phantoms preparation

Solid tissue-like samples were made to simulate the optical properties of biological tissues [25]. The solid samples were made in several steps to create samples enriched with GNPs within samples without GNPs, as can be seen in **Fig. 2**. Initially, the interior samples (15 mm radius) were made by pouring different GNRs concentrations (0.1, 0.07, 0.05 and 0.025 mg/mL), as shown in **Fig. 2 a**. After solidification, the inside samples were placed inside 90mm cell culture plates, as shown in **Fig. 2 b**, where the outside samples solution was added around them to make a homogeneous surface with unmediated interface between the samples with and without GNPs, as can be seen in **Fig. 2 c-d**. At last, to avoid bubbles formation, the combined samples were cooled down in vacuum conditions.

The samples were made with double distilled water (DDW), 1% agarose powder to solidify the solution, 2% IntraLipid (20% Emulsion) as an optical scattering component and 1 \times 10⁻³% India Ink as an optical absorption component [26]. The solutions were blended at 90°C during that the agarose powder was slowly poured in the solution. The samples were made in cell culture plates (30 and 90 mm).

Gold nanorod characterization

The GNPs used in the experiments had a 10 nm diameter and a 37 nm length, purchased from Nanopartz Inc. (Loveland, USA). In **Fig. 3** shown the TEM (CM 100, Philips) image of the GNPs and their normalized

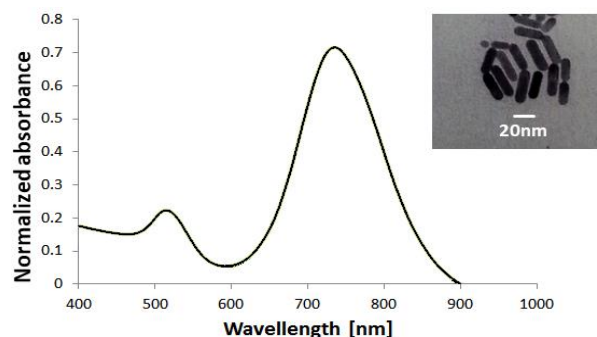


Fig. 3. The normalized absorbance spectra of the GNPs and TEM image of the GNPs having 10 nm length and 37 nm diameter.

absorbance spectrum (ultraviolet-visible spectrometer, Shimadzu, UV1650). The resonance at 530 nm wavelength stems from the LSPR at the narrow size of the GNRs and the resonance at 770 nm wavelength stems from the wide size LSPR.

Experimental results

The heating profile of the phantoms was characterized by illuminating them with a continuous wave NIR laser and the thermal elevation at the center of the laser beam was filmed using the thermal camera. **Fig. 4** shows the temperature change as a function of the GNRs concentration for the illuminated phantoms enriched with GNRs.

As shown in **Fig. 4**, there is a good correlation between temperature elevation and the GNRs concentration. After 10s, for 0.025 mg/mL (the lowest GNRs concentration), a temperature change of around 10°C was observed, while for 0.1 mg/mL (the highest concentration), the temperature elevation after 10s was around 3.5°C. One can see that the linear graphs origins cross the Y-axis (ΔT) slightly above 0°C (although we should expect that for GNRs concentration of 0mg/mL there will not be any temperature change). The small temperature change for samples without GNRs was obtained because an India Ink was added to the samples to simulate the natural optical absorption of healthy tissues. However, the border between the samples with and without GNRs was difficult to discern due to the heat dissipation during the illumination time from the GNRs area outward. To deal with this unwanted effect, the laser illumination was modulated at a frequency of 0.1 Hz in different duty-cycles.

The modulated laser illumination allows cooling of phantoms, and thus decreased the total heat dissipation. However, the exact border detection was difficult to discern due to the global heating of the phantoms during the illumination and the background noise arising from the thermal irradiance of the samples and their environment.

In our previous work this problem was solved by using a simple image processing by subtracting between the thermal maps of the minimum and the maximum temperature at every illumination cycle, and therefore only the areas where the thermal-map was altered were left [22]. However, this method was applied for 20% duty cycle, GNRs concentration of 0.05mg/mL and low noise. In this paper we use special image processing in order to achieve visualization of the border even at highly noised environment and at smaller duty-cycle of 5% and smaller GNRs concentration of only 0.025 mg/mL.

The image processing method that was used is temporally sequenced labeling (TSL) which is rely on the lock-in amplification method for each pixel in the thermal images. The TSL method can cancel image noises, discriminate the data and obtain higher contrast [27,28]. The lock-in amplification technique is used in a variety of applications [29-30]. The TSL method

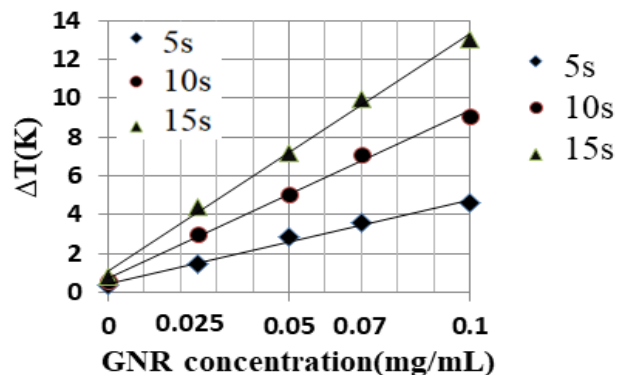


Fig. 4. Temperature elevation as a function of GNRs concentration for three continuous wave illuminations time durations: 5, 10 and 15 sec.

advantages are its capability to recover data from noisy images, and its high sensitivity. The method stems from that even when signal and noise in time domain are indistinguishable, the noise and the signal can be separated in the frequency domain provided that the signal has a specific frequency band without any noise peak. The proposed method modulates the laser source at a wavelength which in correspondence to the GNPs' LSPR at temporal frequency of f_0 . A temporal sequence of intensity images of thermal radiation coming from the sample with GNRs is imaged. The image intensity is equal to the modulated signal and the noise of a time sample:

$$I_t(f) = I_{sig_t}(f_0) + I_{noise_t}(f) \quad (1)$$

where I_t is each image intensity, $t=1 \dots N$ is an index for each image, where N is the total images number, I_{sig} is the signal intensity and I_{noise} is the noise intensity. The noise spectrum is wide, whereas, the signal's temporal frequency components are at the modulated illumination frequency. Therefore, reconstruction of the exact border's spatial location can be achieved by this method. The modulation signal is convolved with each image:

$$I_{conv_t} = I_t(f) * I_{mod_t}(f_0) \quad (2)$$

where I_{conv} is the convolution result and I_{mod} is the modulation signal intensity. * designates convolution operation. The final image I_{TSL} is the average sum of the convolved image:

$$I_{TSL} = \frac{1}{N} \sum_{t=1}^N I_{conv_t} \quad (3)$$

By using the convolution, the signal data is recovered while other contributions from noises that are not at the temporal frequency of the modulated signal, are attenuated.

Fig. 5 a presents a sequence of captured images of the thermal maps for GNRs concentration of 0.025 mg/mL and duty-cycle of 5%. The exact border is not distinguishable. In **Fig. 5 b** one can clearly see that after

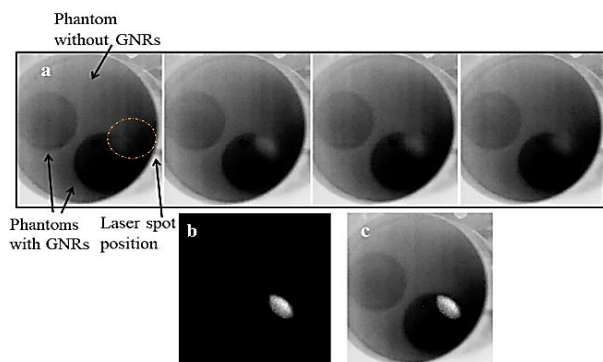


Fig. 5. (a) Sequence of recorded images of the thermal maps, (b) the reconstructed image of the phantom using TSL and (c) the superimposed thermal map before the illumination and before (b).

applying the TSL method, only the areas where the temperature was changed in accordance with the modulated laser illumination were left. These areas are precisely where the illumination come across the GNRs, leading to an improve visualization of the samples with the GNRs border. **Fig. 5c** is the superimposing of the thermal map of the phantom before the illumination and before **Fig. 5b**. There is an overlap between the reconstructed thermal image and the location of the region where the illumination meets the GNRs.

The thermal radiometric camera has a spatial resolution of 0.5 mm, and this is the main factor which limits the proposed method. The two-phase preparation process of the phantoms leads to a diffusion of GNRs to the sample without GNRs. In **Fig. 5 b**, one can see the temperature gradient in the boundary of the sample with GNRs, which is in accordance with the GNRs concentration gradient.

In real tumor, the cancerous cells concentration is smaller in the tumor boundary, and thus the GNRs gradient could mimic a real tumor. The doctor's need for exact boundary detection of tumor during cancer surgery may change for different locations and types of tumors. Generally, resection of an extra healthy tissue reduces the reoccurrence of cancer [31,32]. However, the accuracy of the tumor borders detection is crucial when the tumor is in or is adjacent to neurological systems, and thus it is very critical not to remove an extra tissue. Today, the exact spatial resolution that can be achieved during cancer surgery is about few millimeters [33]. Our technique is supposed to be better than these methods.

Conclusion

The TSL technique is a method for imaging of samples with GNRs which provides an image processing tool to achieve visualization even in noisy environments. In this paper we demonstrate the ability to identify the margins of samples enriched with GNRs with spatial accuracy of better than 0.5mm using the TSL technique. This technique is operational for low GNRs concentration and for low illumination duty cycle. The presented method is very sensitive to thermal changes, and thus by using it in-situ one can significantly decrease the nanoparticles' dose and the illumination power density.

The gold nanoparticles can be specifically targeted to cancer cells. Therefore, the temperature change happens in the cancerous tissue itself, enabling us to differentiate between the non-cancerous and the cancerous tissues. We anticipate this in-vitro method will be an intraoperative photo thermal imaging that will be an assistant to achieve complete tumor resection during cancer surgery even at highly noisy environment.

Acknowledgements

The authors would like to thank Inbar Yariv for samples preparations.

References

- Rhyner, M.N.; Smith, A.M.; Yang, L. Quantum dots and multifunctional nanoparticles: New contrast agents for tumor imaging. *Nanomedicine* **2006**, *1*, 1–9.
- Kircher, M.F.; de la Zerda, A.; Jokerst, J. V; Zavaleta, C.L.; Kempen, P.J.; Mittra, E.; Pitter, K.; Huang, R.; Campos, C.; Habte, F.; et al. A brain tumor molecular imaging strategy using a new triple-modality MRI-photoacoustic-Raman nanoparticle. *Nat. Med.* **2012**, *18*, 829–834.
- Lin, X.Z.; Wu, Z.Y.; Tao, R.; Guo, Y.; Li, J.Y.; Zhang, J.; Chen, K.M. Dual energy spectral CT imaging of insulinoma-Value in preoperative diagnosis compared with conventional multi-detector CT. *Eur. J. Radiol.* **2012**, *81*, 2487–2494.
- Van Dam, G.M.; Themelis, G.; Crane, L.M.; Harlaar, N.J.; Pleijhuis, R.G.; Kelder, W.; Sarantopoulos, A.; de Jong, J.S.; Arts, H.J.; van der Zee, A.G.; et al. Intraoperative tumor-specific fluorescence imaging in ovarian cancer by folate receptor- α targeting: First in-human results. *Nat. Med.* **2011**, *17*, 1315–1319.
- Gerard, I.J.; Kersten-Oertel, M.; Petrecca, K.; Sirhan, D.; Hall, J.A.; Collins, D.L. Brain shift in neuronavigation of brain tumors: A review. *Med. Image Anal.* **2017**, *35*, 403–420.
- Mansfield, J.R.; Gossage, K.W.; Hoyt, C.C.; Levenson, R.M. Autofluorescence removal, multiplexing, and automated analysis methods for in vivo fluorescence imaging. *J. Biomed. Opt.* **2014**, *10*, 41207.
- Hoebe, R.A; Van Oven, C.H.; Gadella, T.W.J.; Dhonukshe, P.B.; Van Noorden, C.J.F.; Manders, E.M.M. Controlled light-exposure microscopy reduces photobleaching and phototoxicity in fluorescence live-cell imaging. *Nat. Biotechnol.* **2007**, *25*, 249–253.
- Carpentier, P.; Violot, S.; Blanchoin, L.; Bourgeois, D. Structural basis for the phototoxicity of the fluorescent protein KillerRed. *FEBS Lett.* **2009**, *583*, 2839–2842.
- Ilovitsh, T.; Danan, Y.; Meir, R.; Meiri, A.; Zalevsky, Z. Cellular imaging using temporally flickering nanoparticles. *Sci. Rep.* **2015**, *5*, 8244.
- Ilovitsh, T.; Danan, Y.; Meir, R.; Meiri, A.; Zalevsky, Z. Cellular superresolved imaging of multiple markers using temporally flickering nanoparticles. *Sci. Rep.* **2015**, *5*, 10965.
- Truong, P.L.; Kim, B.W.; Sim, S.J. Rational aspect ratio and suitable antibody coverage of gold nanorod for ultra-sensitive detection of a cancer biomarker. *Lab Chip* **2012**, *12*, 1102–1109.
- Zhan, Q.; Qian, J.; Li, X.; He, S. A study of mesoporous silica-encapsulated gold nanorods as enhanced light scattering probes for cancer cell imaging. *Nanotechnology* **2010**, *21*, 055704.
- Ankri, R.; Meiri, A.; Lau, S.I.; Motiei, M.; Popovtzer, R.; Fixler, D. Intercoupling surface plasmon resonance and diffusion reflection measurements for real-time cancer detection. *J. Biophotonics* **2013**, *6*, 188–196.
- Shukla, R.; Bansal, V.; Chaudhary, M.; Basu, A.; Bhonde, R.R.; Sastry, M. Biocompatibility of gold nanoparticles and their endocytotic fate inside the cellular compartment: A microscopic overview. *Langmuir* **2005**, *21*, 10644–10654.
- Jain, P.K.; Lee, K.S.; El-Sayed, I.H.; El-Sayed, M.A. Calculated absorption and scattering properties of gold nanoparticles of different size, shape, and composition: Applications in biological imaging and biomedicine. *J. Phys. Chem. B* **2006**, *110*, 7238–7248.

16. Frederix, F.; Friedt, J.-M.; Choi, K.-H.; Laureyn, W.; Campitelli, A.; Mondelaers, D.; Maes, G.; Borghs, G. Biosensing based on light absorption of nanoscaled gold and silver particles. *Anal. Chem.* **2003**, *75*, 6894–6900.
17. Eustis, S.; el-Sayed, M.A. Why gold nanoparticles are more precious than pretty gold: Noble metal surface plasmon resonance and its enhancement of the radiative and nonradiative properties of nanocrystals of different shapes. *Chem. Soc. Rev.* **2006**, *35*, 209–217.
18. McFarland, A.D.; Van Duyne, R.P. Single Silver Nanoparticles as Real-Time Optical Sensors with Zeptomole Sensitivity. *Nano Lett.* **2003**, *3*, 1057–1062.
19. El-Sayed, I.H.; Huang, X.; El-Sayed, M.A. Selective laser photothermal therapy of epithelial carcinoma using anti-EGFR antibody conjugated gold nanoparticles. *Cancer Lett.* **2006**, *239*, 129–135.
20. Jakobsohn, K.; Motiei, M.; Sinvani, M.; Popovtzer, R. Towards real-time detection of tumor margins using photothermal imaging of immune-targeted gold nanoparticles. *Int. J. Nanomed.* **2012**, *7*, 4707–4713.
21. Danan, Y.; Yariv I.; Zalevsky Z.; Sinvani M. Improved Margins Detection of Regions Enriched with Gold Nanoparticles inside Biological Phantom. *Materials* **2017**, *10*, 203.
22. Qian, X.; Peng, X.-H.; Ansari, D.O.; Yin-Goen, Q.; Chen, G.Z.; Shin, D.M.; Yang, L.; Young, A.N.; Wang, M.D.; Nie, S. In vivo tumor targeting and spectroscopic detection with surface-enhanced Raman nanoparticle tags. *Nat. Biotechnol.* **2008**, *26*, 83–90.
23. Ankri, R.; Duadi, H.; Motiei, M.; Fixler, D. In Vivo Tumor detection using diffusion reflection measurements of targeted gold nanorods—A quantitative study. *J. Biophotonics* **2012**, *5*, 263–273.
24. Park, J.H.; Von Maltzahn, G.; Ong, L.L.; Centrone, A.; Hatton, T.A.; Ruoslahti, E.; Bhatia, S.N.; Sailor, M.J. Cooperative nanoparticles for tumor detection and photothermally triggered drug delivery. *Adv. Mater.* **2010**, *22*, 880–885.
25. Dam, J. S.; Pedersen, C. B.; Dalgaard, T.; Fabricius, P. E.; Aruna, P.; Andersson-Engels, S. Fiber-optic probe for noninvasive real-time determination of tissue optical properties at multiple wavelengths. *Appl. Opt.* **2001**, *40*, 1155–1164.
26. Cubeddu, R.; Pifferi, A.; Taroni, P.; Alessandro, T.; Valentini, G. A solid tissue phantom for photon migration studies. *Phys. Med. Biol.* **1997**, *42*, 1971–1979.
27. Wolfson, R. The lock-in amplifier: A student experiment. *Am. J. Phys.* **1991**, *59*, 569–572.
28. Bhagyajyoti, J.; Sudheer, L. Review on Lock-in Amplifier. *Int. J. Sci. Eng. Technol. Res.* **2012**, *1*, 40–45.
29. Sonnaillon, M. O.; Bonetto, F. J. A low-cost, high-performance, digital signal processor-based lock-in amplifier capable of measuring multiple frequency sweeps simultaneously. *Rev. Sci. Instrum.* **2005**, *76*, 24703.
30. Murphy, M. K.; Clyburn, S. a.; Veillon, C. Comparison of lock-in amplification and photon counting with low background flames and graphite atomizers in atomic fluorescence spectrometry. *Anal. Chem.* **1973**, *45*, 1468–1473.
31. Rhyner, M. N.; Smith, A. M.; Yang, L. Quantum dots and multifunctional nanoparticles: new contrast agents for tumor imaging. **2006**, *1*, 1–9.
32. Kircher, M. F.; de la Zerda, A.; Jokerst, J. V.; Zavaleta, C. L.; Kempen, P. J.; Mittra, E.; Pitter, K.; Huang, R.; Campos, C.; Habte, F.; Sinclair, R.; Brennan, C. W.; Mellinghoff, I. K.; Holland, E. C.; Gambhir, S. S. A brain tumor molecular imaging strategy using a new triple-modality MRI-photoacoustic-Raman nanoparticle. *Nat. Med.* **2012**, *18*, 829–34.
33. Neeman, Z.; Wood, B. J. Radiofrequency ablation beyond the liver. *Tech. Vasc. Interv. Radiol.* **2002**, *5*, 156–163.